Article:
Cao, L, Cochrane, RF and Mullis, AM (2015) Lamella structure formation in drop-tube processed Ni-25.3 at.% Si alloy. Journal of Alloys and Compounds, 615 (S1). S599 - S601. ISSN 0925-8388

https://doi.org/10.1016/j.jallcom.2013.11.233

Lamella structure formation in drop-tube processed Ni-25.3 at.% Si alloy

Leigang Cao[1], Robert F. Cochrane[1], Andrew M. Mullis[1,a]

[1]Institute for Materials Research, University of Leeds, Leeds LS2-9JT, UK

[a]Corresponding author: a.m.mullis@leeds.ac.uk

Abstract

Rapid solidification experiments have been performed on an Ni-25.3 at.% Si alloy using drop tube techniques. The dominant phase formed is found to be $Ni_{25}Si_9$, with $Ni_{31}Si_{12}$ and β_1-Ni_3Si also being present. SEM and TEM analysis revealed a novel eutectic structure consisting of lamellar of metastable $Ni_{25}Si_9$ and β_1-Ni_3Si, the width of these being around 200 nm and 20 nm respectively. This result indicates that there is a possible eutectic reaction for the $Ni_{25}Si_9$ and β_1-Ni_3Si phases existing in the metastable phase diagram.

Keywords: Rapid solidification processing; Metastable phase formation; Lamellar structure

1. Introduction

The intermetallic phase βNi_3Si is of interest because it displays excellent high temperature oxidation resistance and high hardness at elevated temperature [1-3]. However, like many other intermetallics, it is brittle at room temperature, which restricts its application owing to fabricating difficulty [3,4]. One potential route to overcoming this difficulty is non-equilibrium processing via rapid solidification, with the resulting fine grain structure and the presence of anti-phase domains increasing room temperature ductility [5].

Several rapid solidification studies have been carried out on the Ni rich end of the Ni-Si system, mainly concentrating on the eutectic alloy, Ni-21.4 at.%. Liu et al. and Lu et al [6,7] achieved undercoolings up to 550 K by using a glass fluxing and cyclic superheated method, observing a microstructural evolution from regular lamellar eutectic to superfine anomalous eutectic, via a range of dendritic morphologies. Conversely, a study by Goetzinger et al. [8] attained a regular eutectic microstructure for $\Delta T < 30$ K, which was then progressively replaced by anomalous eutectic structures as the undercooling increased, with the transition being complete for $\Delta T > 150$ K. One common feature here was that only α-Ni and β-Ni_3Si were formed in these alloys, a result also found in drop tube experiment by Çadırlı et al. [9]. However, by quenching the undercooled sample onto a chilled substrate Leonhardt et al.[10] observed the formation of the metastable phase $Ni_{25}Si_9$, as did Dutra et al.[11] using a melt-spinning technique. Fig. 1 shows the Ni-rich end of the Ni-Si phase diagram including the metastable $Ni_{25}Si_9$ phase.

Ahmad et al.[13] used a fluxing method to undercool a Ni-25.2 at.% Si alloy in an attempt to directly access the β-Ni_3Si phase (the stability fields being 25.0-26.1 at.% Si for β_2/β_3 and 22.6-24.5 at.% Si for β_1). However, despite obtaining the required undercooling they found that they were unable to obtain single phase β-Ni_3Si. Instead they observed a eutectic structure comprising alternating lamellae of single phase γ-$Ni_{31}Si_{12}$ and supersaturated α-Ni lamellae which had decomposed to β_1-Ni_3Si and α-Ni via a eutectoid reaction. A small amount of $Ni_{25}Si_9$ was also formed in the final solidified sample. In this paper, an alloy of the same notional composition (Ni- 25 at.% Si) was chosen and drop tube technique was employed to research the phase formation and microstructure evolution.

2. Experimental

The alloy of composition Ni-25.3 at.% Si, was produced from its elemental constituents (purity = 99.99% Ni, 99.999% Si) by arc-melting under a protective argon atmosphere, this process being repeated 5 times to ensure uniform mixing of the final sample.

Rapid solidification was affected using a 6.5 m drop-tube, which was filled to a pressure of 50 kPa with dried, oxygen free N_2 gas, having previously been flushed multiple times with N_2 and evacuated to a pressure of 4×10^{-7} Pa. The sample was then loaded into an alumina crucible with 3 laser drilled holes (300 μm diameter) in the base, which was heated by induction of heating of a graphite susceptor. Temperature determination was by means of an R-type thermocouple inside the melt crucible. When the desired superheat was achieved the melt was ejected by pressuring the crucible with 400 kPa of N_2 gas.

The resulting alloy particles were sieved into standard size ranges and then hot mounted using Transoptic resin for XRD detection, or carbon filled conductive resin for SEM analysis. The mounted samples were ground using

a series of progressively finer SiC papers starting with 240, 400, 800 and lastly 1200 grit, with optical microscopy being used to check the quality of the surface finish at each stage. Once the samples were appropriately ground they were polished using 6 μm, 3 μm, 1 μm and 0.25 μm diamond paste. The samples were washed using dilute detergent and methanol and then dried using hot air between each polishing step. The composition of the well polished samples was characterized using Scanning Electron Microscopy (SEM) with an energy dispersive spectrometer (EDS). To reveal the microstructure the well polished samples were etched using here a mixture of Hydrofluoric Acid (5ml), Hydrogen Peroxide (5ml) and water (10ml) to obtain SEM high resolution images. Lamella samples, taken from areas of interest within the samples, were extracted using FIB milling for subsequent characterisation using Transmission Electron Microscopy (TEM).

3. Results and discusstions

EDX analysis of the drop tube solidified particles was carried out to check the composition, which were measured within the range 24.0-26.0 at.% for Si. X-ray diffraction analysis was also performed to identify the phases present and example diffraction patterns for larger (300-500 μm), and finer (106-150 μm) particles are shown in Fig. 2. The resulting diffraction patterns show the presence of three phases: $Ni_{31}Si_{12}$, β_1-Ni_3Si, and metastable $Ni_{25}Si_9$, this latter being the dominant phase present. The structure of metastable phase $Ni_{74}Si_{26}$ is a stacking variant of $Ni_{25}Si_9$, and it is very difficult to distinguish this two phases due to their similar dominant diffraction peaks [14]. Here we just refer $Ni_{25}Si_9$ for discussion. This metastable phase formation we attribute to the high undercooling induced by the high cooling rate and its retention at room temperature to the high cooling rate experienced during solidification processing. We note that the stoichiometry of the $Ni_{25}Si_9$ phase is quite close to the initial experimental composition which would reduce the solute diffusion necessary for its formation, in line with the observations of [13].

Microstructural analysis was carried out using SEM, with highly regular lamellar nanostructures being observed in particles with diameters in the range 106-850 μm. One such example microstructure, taken from a particle in the 300-500 μm sieve fraction, is shown in Fig. 3. In order to determine the origin of this lamella structure, fine lamellae TEM samples (12 × 8 μm) have been taken using the Focus Ion Beam technique. A bright field TEM micrograph is shown in Fig 4(a), which shows alternating regular lamellae comprising wide (≈ 200 nm) and narrow (≈ 20 nm) bands. From Fig 4(a) it is clear that the thin bands are continuous with, and therefore the same phase as, the single phase region embedded within the lamella structure. A selected area diffraction pattern confirms that this single phase region, and therefore the thin lamellae are the intermetallic phase β_1-Ni_3Si, as shown in fig 4(b). A similar selected area diffraction pattern analysis confirms that the wide lamellae are likely to be $Ni_{25}Si_9$, as shown in Fig 5. In addition to the widespread 2-phase structure reported in Fig. 3-4, some particles show small regions in which $Ni_{25}Si_9$ appears to be overgrown by $Ni_{31}Si_{12}$.

The formation of the metastable phase $Ni_{25}Si_9$ has been observed previously [10,11], however the fine co-growth structure observed here has not been reported before. As can be seen from the phase diagram, there are two high temperature form of β-phase, disordered β_3 and ordered β_2. Based on the model of Kasperovich et al. [15], the estimated average cooling rates for 300-500 μm and 106-150 μm particles are 1300 K s^{-1} and 10400 K s^{-1} respectively. Such high cooling rate would be expected to favour the formation of β_3 or β_2 phases, with their subsequent decomposition giving a possible formation route for the observed β_1-$Ni_{25}Si_9$ lamellar structure. However, XRD analysis failed to indicate the presence of any β_3 and β_2 in of our samples, from which we think this formation route is unlikely, as some residual β_2/β_3 would be expected to remain at the highest cooling rates, particularly as Ahmad et al [13] observed extensive retained β_3 in fluxed samples in which a cooling rate < 10 K s^{-1} would be expected. Consequently, we conjecture that the observed lamellar structure formed as a result of a hitherto unobserved eutectic between β_1 and $Ni_{25}Si_9$, with the present experimental composition close to the eutectic composition.

This solidification pathway is not only different from the prediction of the equilibrium phase diagram, but also different from the results of Ahmad et al [13], who observed a coarse lamella structure consisting of $Ni_{31}Si_{12}$ and a Ni rich phase. Generally, lamellar eutectic growth at low undercooling [8,16] gives way to anomalous eutectic structures as the undercooling increases [17]. However, this is not inconsistent with the result in present paper, because high cooling rate and undercooling are the determinant factors for the nucleation and growth of metastable $Ni_{25}Si_9$ phase. Moreover, Ahmad et al [13] observed exceptionally low growth velocity and the retention of lamellar eutectic structures in Ni- 25 at.% alloy, even at undercoolings of 160 K. This they attributed to an anomalous high viscosity, and consequently a depressed atomic mobility in the undercooled melt. This would in turn lead to the very fine structures observed here and a tendency to favour solid phases which were not very different in composition to that of the undercooled parent melt. In addition, according to the metastable liquidus line (Fig.1) shown by Leonhardt et al.[10], the possible eutectic structure would be $Ni_{25}Si_9$ and αNi in deep non-equilibrium process. The discovery here of $Ni_{25}Si_9$ and β_1-Ni_3Si eutectic would

imply that the metastable liquidus line of $Ni_{25}Si_9$ would be dropping much more steeply with regard to the formation of β_1-Ni_3Si phase.

4. Conclusions

Rapid solidification of the Ni-25 at.% Si hypereutectic alloy resulted in a regular eutectic microstructure consisting of metastable phase $Ni_{25}Si_9$ and β_1-Ni_3Si, with thickness being about 200 nm and 20 nm respectively. This result indicates that there is a metastable eutectic reaction between $Ni_{25}Si_9$ and β_1-Ni_3Si, expected for Si composition between 24.5 at.% (β_1-Ni_3Si) and 26.47 at.% ($Ni_{25}Si_9$).

References

[1] P.H. Thornton and R.G. Davies, The temperature dependence of the flow stress of gamma prime phases having the $L1_2$ structure. Metall. and Mater. Trans. B 1(1970) 549-550.
[2] E.M. Schulson, L.J. briggs, and I. Baker, The strength and ductility of Ni_3Si. Acta Metall. 38 (1990) 207-213.
[3] N.S. Stoloff, C.T. Liu, and S.C. Deevi, Emerging applications of intermetallics. Intermetallics, 8 (2000) 1313-1320.
[4] R.L. Fleischer, High-strength, high-temperature intermetallic compounds. J. Mater. Sci. 22 (1987) 2281-2288.
[5] D.M. Herlach, Non-equilibrium solidification of undercooled metallic melts. Mater. Sci. and Eng., R. 12 (1994) 177-272.
[6] F. Liu, et al., Competitions incorporated in rapid solidification of the bulk undercooled eutectic $Ni_{78.6}Si_{21.4}$ alloy. J. Mater. Res. 22(2007) 2953-2963.
[7] Y. Lu, et al., Microstructure and hardness of undercooled $Ni_{78.6}Si_{21.4}$ eutectic alloy. J. Alloys Compd. 490(2010) L1-L4.
[8] R. Goetzinger, M. Barth, and D.M. Herlach, Mechanism of formation of the anomalous eutectic structure in rapidly solidified Ni-Si, Co-Sb and Ni-Al-Ti alloys. Acta Mater. 46 (1998) 1647-1655.
[9] E. Çadırlı, D.M. Herlach, and T. Volkmann, Characterization of rapidly solidified Ni-Si and Co-Al eutectic alloys in drop tube. J. Non-Cryst. Solids, 356 (2010) 461-466.
[10] M. Leonhardt, W. Löser, and H.G. Lindenkreuz, Metastable phase formation in undercooled eutectic $Ni_{78.6}Si_{21.4}$ melts. Mater. Sci. Eng., A, 271 (1999) 31-37.
[11] A.T. Dutra, et al., Microstructure and metastable phase formation in a rapidly solidified Ni–Si eutectic alloy using a melt-spinning technique. J. Alloys Compd. 381(2004) 72-76.
[12] T.B. Massalski and H. Okamoto. Binary Alloy Phase diagrams. second ed., ASM International, 1990.
[13] R. Ahmad, R.F. Cochrane, and A.M. Mullis, The formation of regular αNi-γ($Ni_{31}Si_{12}$) eutectic structures from undercooled Ni–25 at.% Si melts. Intermetallics, 22(2012) 55-61.
[14] M. Ellner, et al., Einige strukturelle untersuchungen in der mischung $NiSi_N$. J. Less Common Met. 66 (1979) 163-173.
[15] G. Kasperovich, et al., Microsegregation during Solidification of an Al-Cu Binary Alloy at Largely Different Cooling Rates (0.01 to 20,000 K/s): Modeling and Experimental Study. Metall. Mater. Trans. A, 39(2008) 1183-1191.
[16] L.Q. Xing, D.Q. Zhao, and X.C. Chen, Solidification of undercooled Ni-32.5 wt% Sn eutectic alloy. J. Mater. Sci. 28 (1993) 2733-2737.
[17] C.R. Clopet, R.F. Cochrane, and A.M. Mullis, Spasmodic growth during the rapid solidification of undercooled Ag-Cu eutectic melts Appl. Phys. Lett. 102(2013) 031906 - 031906-4.

Fugure list:

Fig. 1. Ni-rich portion of the Ni-Si phase diagram [12]. The dashed lines indicate the metastable $Ni_{25}Si_9$ phase. Dotted lines T_L and T_S are metastable extensions of liquidus and solidus lines of the $Ni_{25}Si_9$ phase [10].

Fig. 2. X-Ray diffraction traces for 106-150 and 300-500 μm, Ni-25.3 at.% Si drop tube particles. Two of the diffraction diagrams are almost the same, showing a large fraction of metastable $Ni_{25}Si_9$/$Ni_{74}Si_{26}$ existing in both size fractions, in addition to $Ni_{31}Si_{12}$ and β_1-Ni_3Si phases. The peaks corresponding to $Ni_{25}Si_9$/$Ni_{74}Si_{26}$ (♦), $Ni_{31}Si_{12}$ (●) and β_1-Ni_3Si (♠) are labelled.

Fig. 3. High resolution SEM micrograph from one Ni - 25 at% Si alloy drop tube particle with size being 500-300 μm, showing typical lamella structure.

Fig. 4. (a) TEM bright field micrographs from the FIB sample, which indicates that the thin layer in the lamella structure and the bulk dark phase are same phase; (b) The selected area electron diffraction pattern for the bulk dark phase in (a), identifying the single phase region (and therefore the thin lamella) as β_1-Ni_3Si.

Fig. 5. TEM bright field micrograph of the lamella structure. Inset diffraction pattern is obtained from the lamella area, in which the corresponding d-sapcing is 0.9264 nm. Comparing with the standard diffraction data of phases $Ni_{25}Si_9$ and $Ni_{31}Si_{12}$, this data indicated that wide layer phase of the lamella structure is metastable phase $Ni_{25}Si_9$.

Figure 1

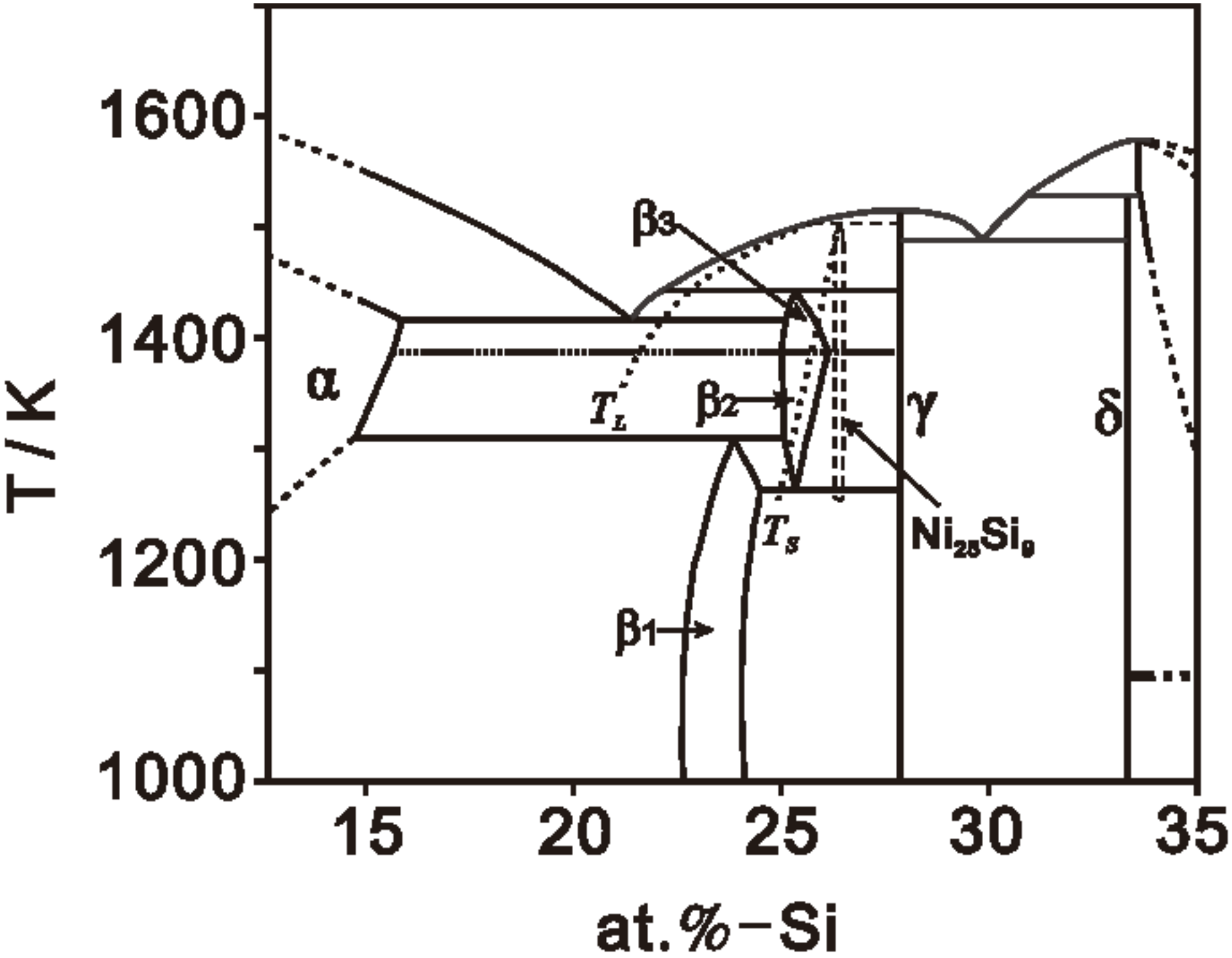
1600
1400
1200
1000
T / K
15
20
25
30
35
at.%−Si
α
β3
β2
β1
T_L
T_S
γ
δ
$Ni_{25}Si_9$

Figure 2

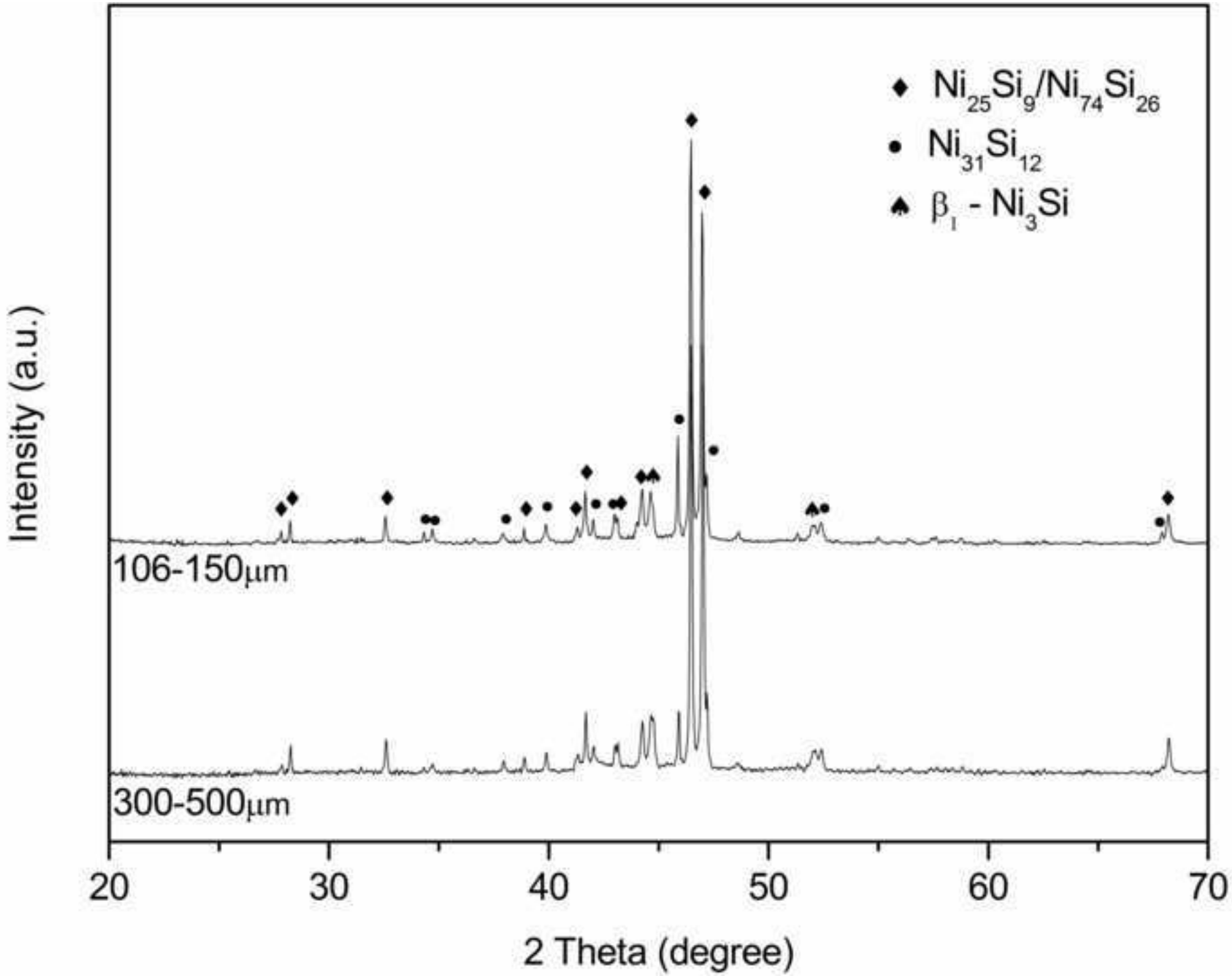
Ni25Si9/Ni74Si26
Ni31Si12
β1 - Ni3Si
106-150μm
300-500μm
Intensity (a.u.)
20
30
40
50
60
70
2 Theta (degree)

Figure 3

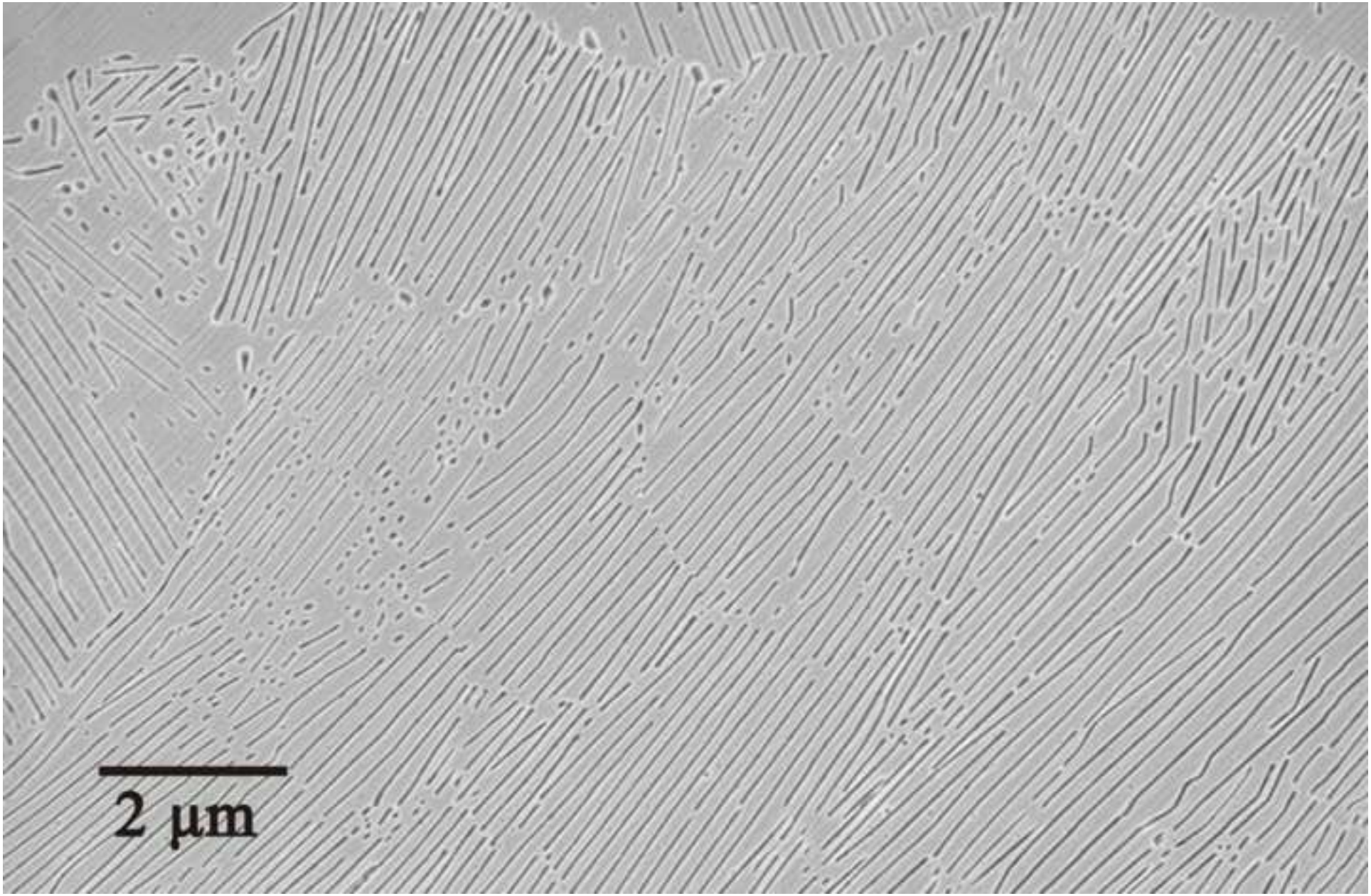

Figure 4 (a)

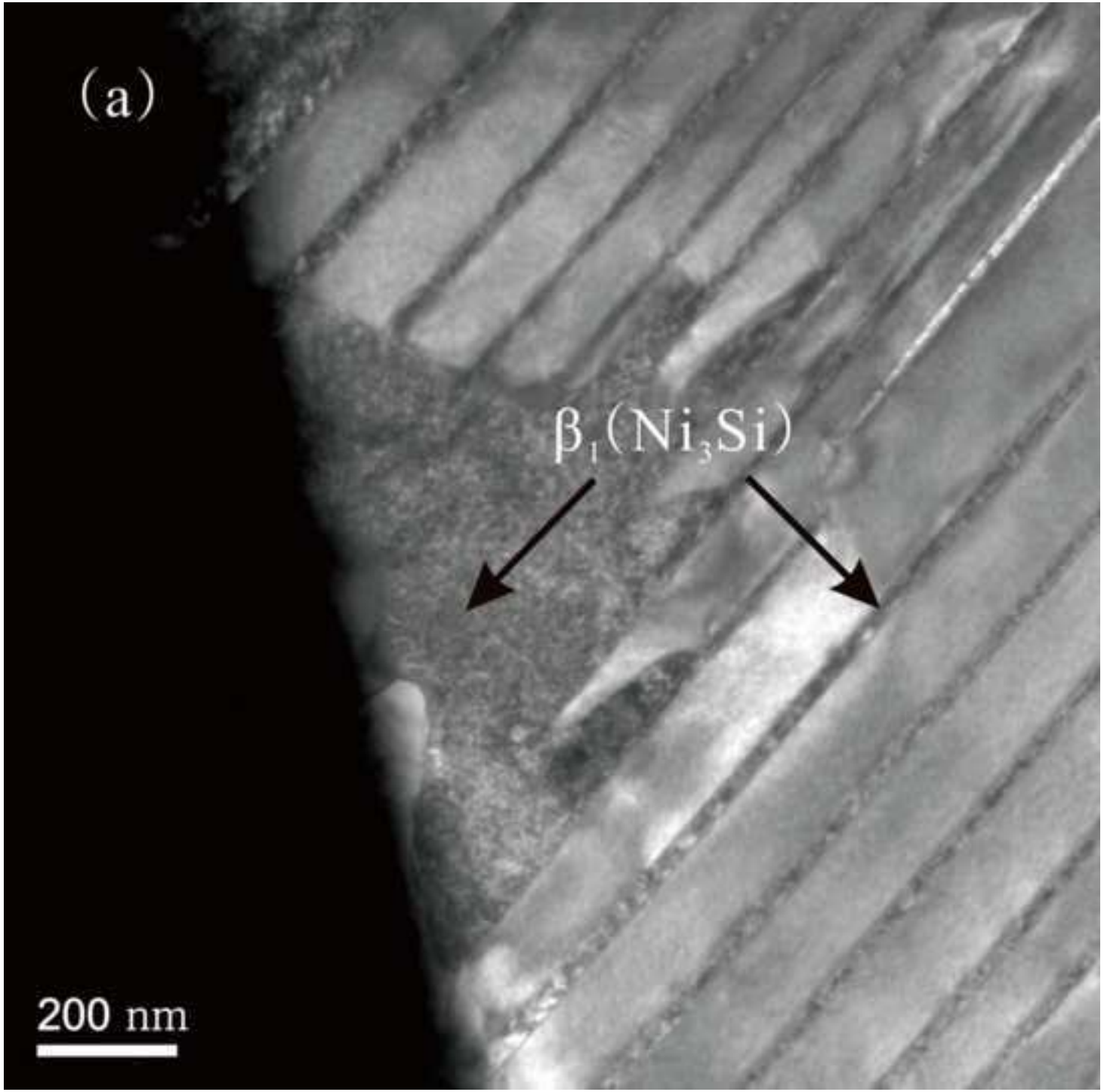

Figure 4 (b)

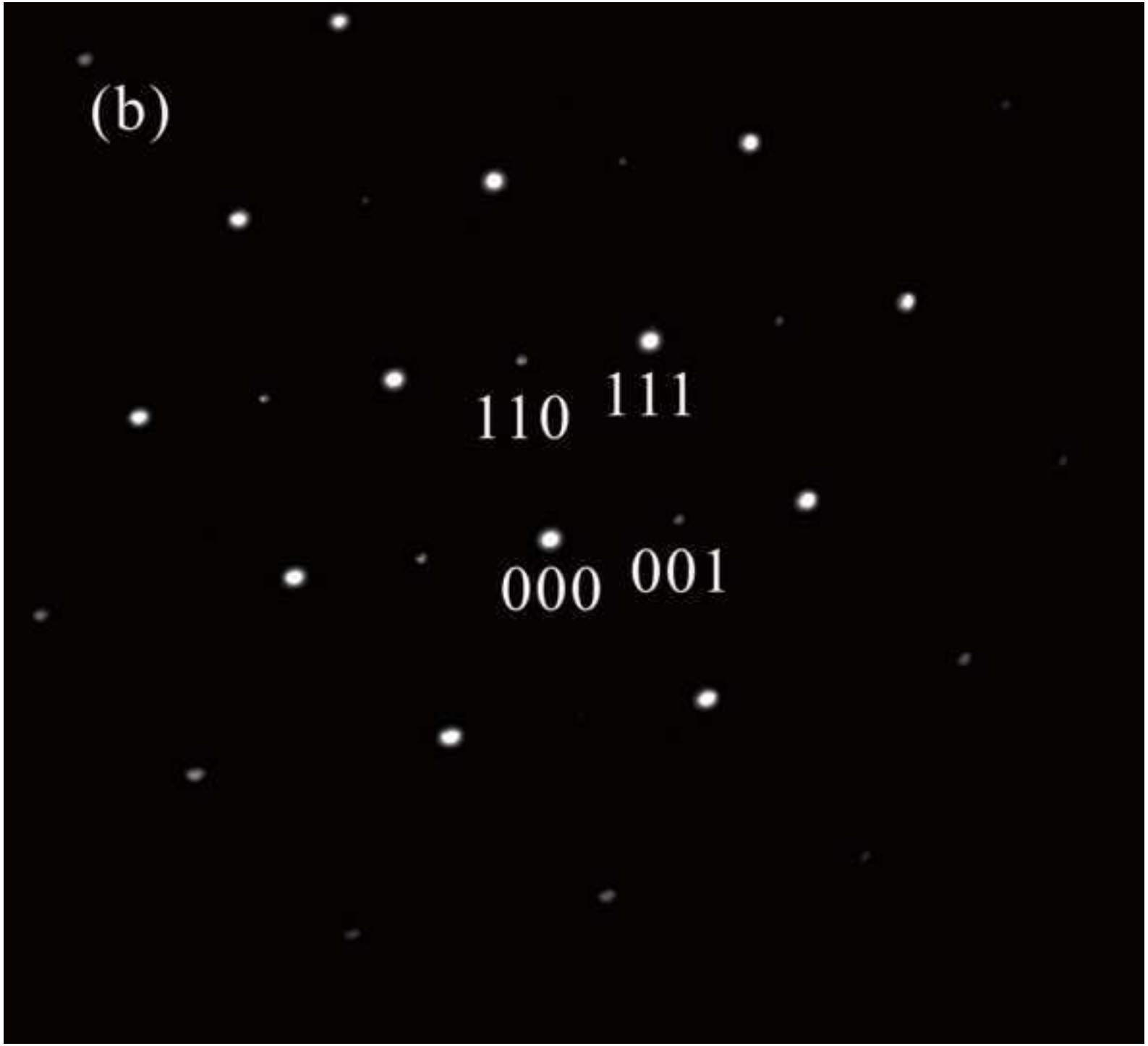

Figure 5